Egyptian Journal of Pure and Applied Science

Uranium Mineralization and Rare Metals Associating Shear Zone in the Younger Granites at Wadi Akhdar Area, Southwestern Sinai, Egypt

Ismail A. El Akeed*

Nuclear Materials Authority, P.O. Box – 530 Maadi, Cairo, Egypt

ARTICLE INFO

Article history:
Received 19 October 2014
Accepted 24 November 2014

Keywords:
Uranium Mineralization;
Rare Metals;
Shear Zone;
Spectrometry;
Hydrothermal alteration;
Granite;
Wadi Akhdar;
Sinai;
Egypt.

ABSTRACT

The Wadi Akhdar area is made up mainly of younger granites (syeno-, and monzogranites) intruding granodiorite with sharp contacts. These granites are dissected by swarms of shear zones, one of which exists along the contact between the two types of granites. The shear zones trend NW-SE and consist of closely spaced fractures along which alteration products pegmatitic dykes and pockets and hydrothermal veins are recoded. Detailed spectrometric and mineralogical studies are carried out on the shear zone. The geochemical characteristics of the monzogranite indicate derivation from peraluminous magma having features of the I-type granite and emplaced in volcanic arc tectonic environment. The syenogranite (A-type granite) originated from a magma which has peraluminous to metaluminous characters and emplaced in within-plate tectonic setting. The wide ranges of major and trace element compositions of these two granite types are generally attributed to variations of source compositions, tectonic environments and models of emplacement which explain the petrogenesis of a particular suite. The spectrometric study of the shear zone reveals that it has high uranium-thorium concentrations. In this mineralized shear zone, seven important uranium and uraniferous minerals together with some rare metals were detected. These minerals include uraninite, uranpyrochlore, davidite-(Ce), liandratite, walpurgite, thorogummite and weeksite. The proposed origin of these minerals is hydrothermal since they occur within pegmatitic dykes and pockets and hydrothermal veins as well as along the fracture planes associated with the alteration products such as silicification, hematitization epidotization and kaolinization hematitization epidotization and kaolinization.

Introduction

The Wadi Akhdar area is characterized by the presence of granitoid rocks that include older and younger granites. The older granite is represented mainly by granodiorite while the younger granites are dominated by monzo- and syenogranites. The younger granites of south Sinai were classified according to their field relationships and petrological characteristics into two groups [1-6]. These two groups correspond to phase II and phase III of the Egyptian younger granites recognized by Akaad et al. [7], Akaad and Nowier [8] and Rogers and Greenberg [9]. These granites have a wide compositional range as they originated from peraluminous to peralkaline magma and were formed either as suturing or post-orogenic and emplaced in an extensional environment; i.e. evolved in a within–plate environment [1,5,10-12]. El Tokhy [13] concluded that the main fault trends in the area are NNW-SSE (Red Sea trend), NE-SW and N-S. Most of these faults are of the normal type. Ibrahim [14] stated that the uranium- and thorium-bearing minerals were carried by hydrothermal solutions and pneumatolytic gases and re-precipitated along the faults of the younger NW trend.

The contact of the monzogranite with syenogranite is marked by the presence of one mineralized shear zone and comprises sub-parallel pegmatitic dykes and quartz veins. This shear zone was highly affected by hydrothermal solutions. It, together with its pegmatitic dykes and pockets as well as hydrothermal veins, were highly enriched in some important metal cations the concentrations of which reached a limit that permitted the formation of their own minerals.

* Corresponding author.
E-mail address: elakeed68@yahoo.com

The aim of this work is to study the geochemical and mineral characteristics of the uranium minerals and their assemblages that contain important metals in the mineralized shear zone. This includes the study of the geochemical behavior of selected major and trace elements to determine the type of the source magma. Also, the tectonic setting and the petrogenesis of the younger granites are investigated. The detailed spectrometric investigation of the anomalous shear zone was performed to determine its contents of uranium and thorium. In addition, the aim comprises the recognition and identification the uranium and/or thorium minerals as well as the associated rare metal-bearing minerals by using X-ray diffraction (XRD) and Environmental Scanning Electron Microscope (ESEM) supported by an EDAX unit which were conducted at the laboratories of the Nuclear Materials Authority (NMA), Egypt.

Geologic setting

The studied Wadi Akhdar area is located between Longitudes 33° 44' 19" and 33° 48' 08" E and Latitudes 28° 45' 50" and 28° 51' 33" N. It contains exposures of granodiorites and younger granites (Fig. 1).

The younger granites are classified into two phases; namely: monzogranite and syenogranite. The monzogranite outcrops exist at the eastern part of the area and display low to moderate relief. They are whight pink, medium- to coarse- grained and highly weathered. The syenogranite represents the youngest intrusive magmatic event recognized in the area. Its exposures have moderate to high relief and form oval-shaped body extending along the NW-SE direction. It extends out west of the mapped area. The rocks are pink and, in places, showing exfoliation of spheroidal bodies highly weathered display in highly jointed and sheared.

One shear zone exists in the study area extending N 30^0 W along the two sides of the contact between the two phases of younger granites. This shear zone has 70m length and 20m width. It is located in the NW-SE dip-slip fault zone. The detailed spectrometric survey of the shear zone reveals its high content of radioactive elements (Th and U). It is characterized by the presence of several mineralized pegmatitic dykes and pockets together with swarms of hydrothermal veins and aplite dykes (Fig. 2 A to D). These veins and dykes trend

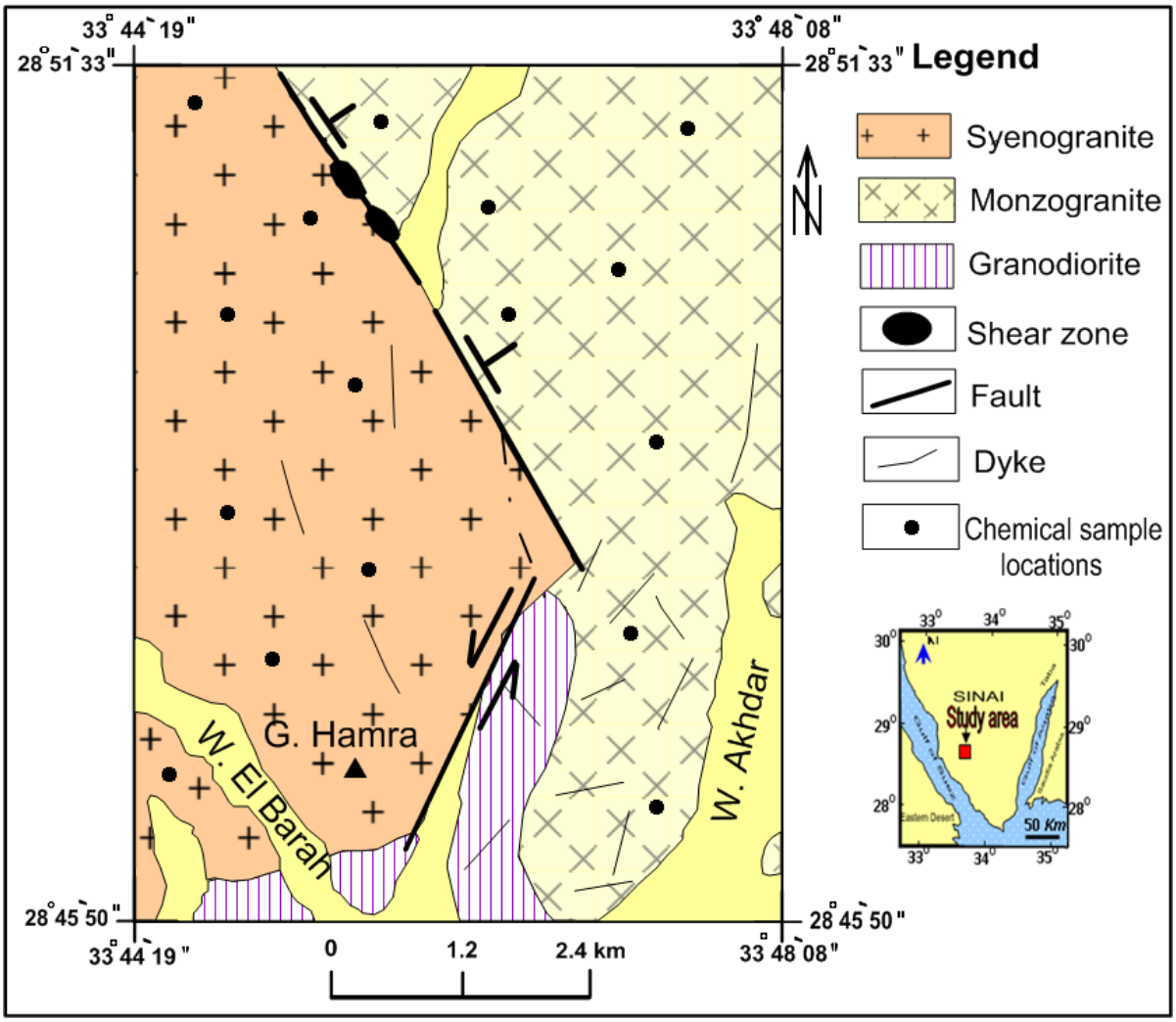

Fig. (1): Location and geologic maps of the studied Wadi Akhdar area.

mainly N30ºW and range in thickness from a few centimeters to 80cm. The fractures and joints developed in the shear zone acted as pathways for the solutions responsible for precipitating uranium minerals and their associations. These minerals are observed as disseminations or impregnations along the fracture planes existing along the shear zone (Fig. 2 E and F). The fault plane is characterized by slickensides stained with iron oxides such as hematite. Fault gauge and wall-rock alterations are also observed as hematitic and kaolinitic materials (Fig. 3 A and B). Alteration processes such as silicification, hematitization, epidotization and kaolinization have their prints along the shear zone.

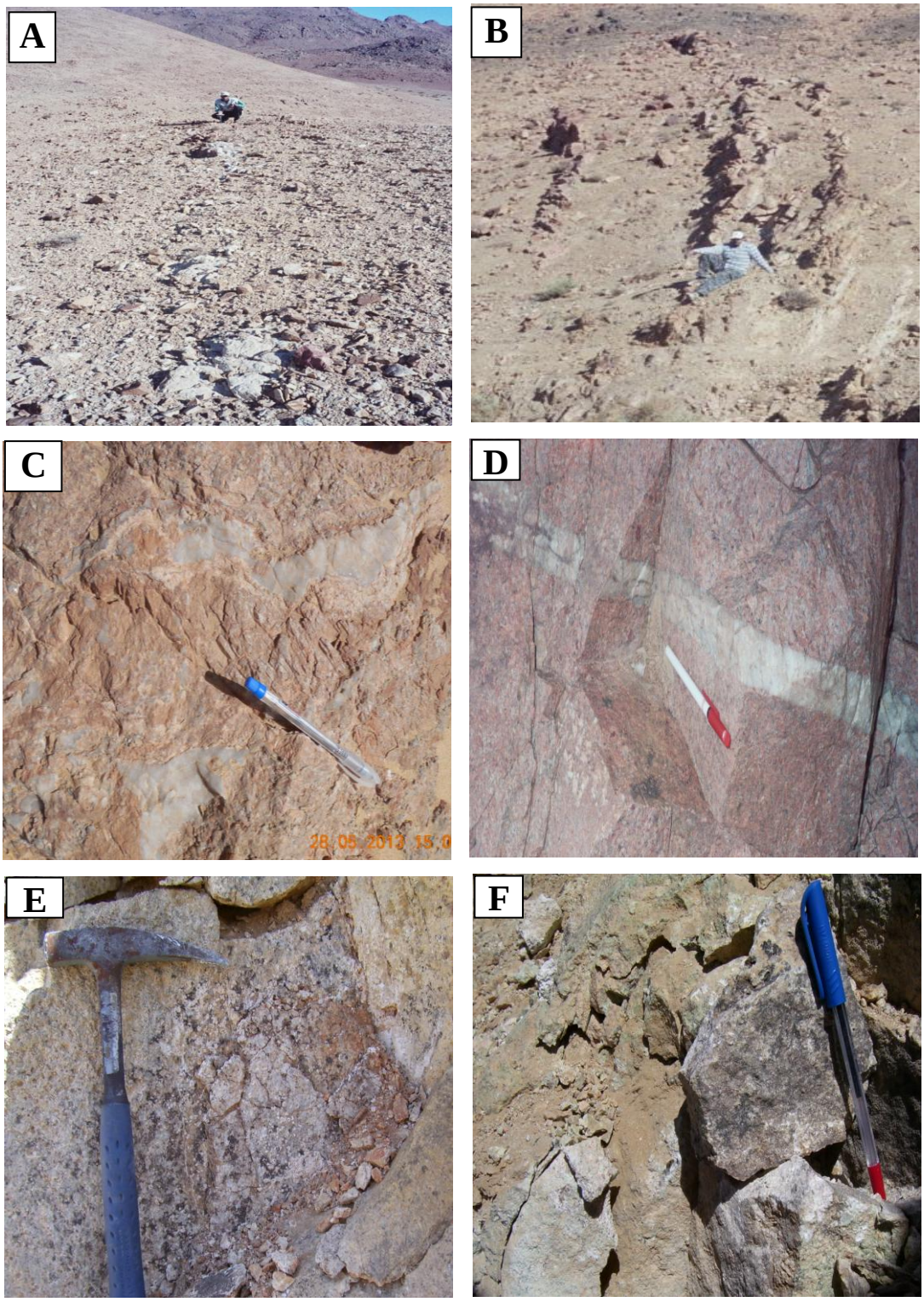

Fig. (2): Field photographs showing the mineralized pegmatitic dykes (A & B) and pockets (C), and a hydrothermal vein (D). Mineral disseminations (E) and mineral stainings and impregnations on the fracture planes (F).

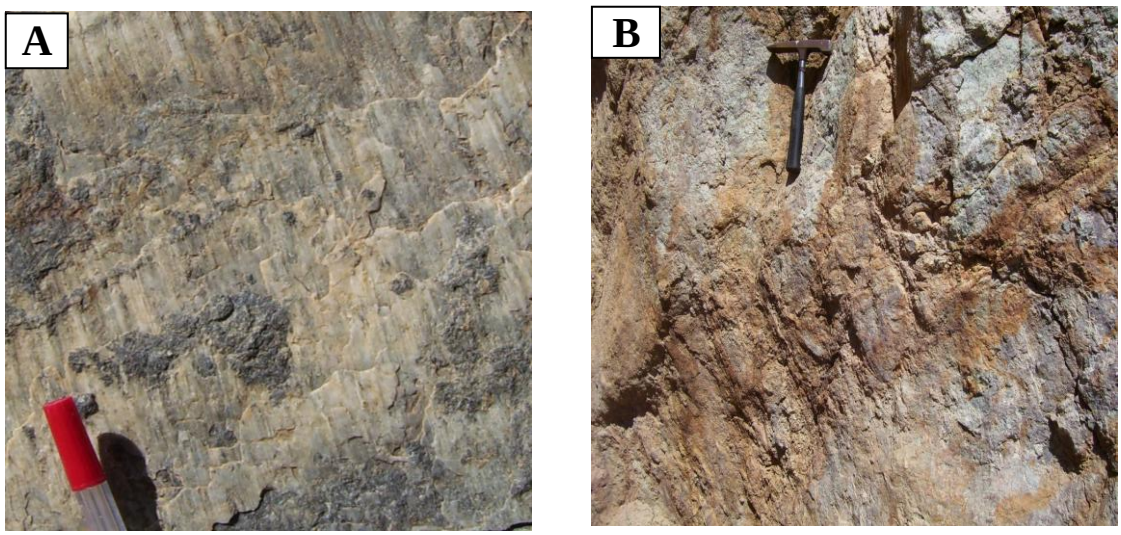

Fig. (3): Field photographs showing the slickensided fault surface (A) and fault gauge and wall-rock alterations existing as hematitic and kaolinitic materials (B).

Methodology

Geochemical analysis was performed on 16 fresh samples representatives of the monzogranite (8 samples) and syenogranite (8 samples). They were analyzed for their major oxides and selected trace elements. The chemical analyses were carried out in the laboratories of the Egyptian Nuclear Materials Authority (NMA), Cairo, Egypt. The major oxides were measured using the conventional wet chemical technique adopted by Shapiro and Brannock [15] and modified by El-Reedy [16]. The concentration of SiO_2, TiO_2, Al_2O_3 and P_2O_5 were determined using UNICAM UV2/100 spectrophotometer, while those of CaO, MgO, Fe_2O_3 and FeO were measured gravimetrically. The contents of Na_2O and K_2O were determined using PFP–7. Flame Photometer flame while MnO was analyzed using the GBC 932/933 Atomic Absorption Spectrometer. On the other hand, the concentrations of trace elements were determined using X-ray fluorescence analysis. A detailed surface ground spectrometric survey was carried out on the anomalous zone and in part on the surrounded monzogranite and syenogranite country rocks to measure the concentrations of eU and eTh. The measurements were conducted along six equally-spaced N-S trending profiles which are arranged at an oblique angle to the strike of the highly anomalous zone. The interval between the profiles and also that between the stations along their strikes was 10m. In this grid, 67 stations were measured. The measurements were carried out using Multichannel Gamma Ray Spectrometer Rs-230. Thirty samples were collected from the mineralized shear zone and the fresh host granitic rocks. They were subjected to heavy mineral separation. Each samples was crushed, sieved and its heavy mineral constituents were separated using bromoform (sp. g. = 2.82gm/cm^3) followed by methylene iodide (sp. g. = 3.325gm/cm^3). The obtained heavy fractions were subjected to magnetic separation. The mineral composition of the picked grains was determined using X-ray diffraction (XRD) and their morphological characteristics and chemical composition were assessed using the Environmental Scanning Electron Microscope (ESEM) supported by EDAX unit. The mineralogical investigation was carried out in the laboratories of the Egyptian Nuclear Materials Authority (NMA), Cairo, Egypt.

Results

1- Geochemistry

The chemical composition and CIPW-norms of the collected granitic samples are given in tables (1) and (2).

The averages of the major oxides in the two types of granite are presented in **Figure (4)**. It shows that the concentrations of TiO_2, Al_2O_3, Fe_2O_3, MnO, MgO, CaO, and P_2O_5 are slightly higher in the monzogranite as compared with syengranite, while those of SiO_2, FeO, Na_2O and K_2O are slightly lower. Evidently, the concentrations of these oxides are controlled by the mineral constituents of the two granite types, where the syenogranite contains more potash feldspars than the monzogranite. The sum of the other oxides (Fe_2O_3, FeO, CaO, MnO, MgO, and P_2O_5) is higher in the monzogranite which is attributed to their enrichment in mafic minerals such as biotite and hornblende.

The comparison between the averages of trace element concentrations in the two granite types is shown in **Figure (5)**. It shows that the monzogranite is enriched in Co, Pb, Ba, Sr, Ni, V, and Ga as compared with the syenogranite. These elements are mostly contained in the early fractionated ferromagnesian mineral phases, so their concentrations are higher in the monzogranite. The contents of Cu, Zn, Rb, Nb, Zr, Y and Cr are higher in the syenogranite than the monzogranite. This can be explained by the fact that they increase with the increase of the magmatic light fractions. Sr is lower in monzogranite than the syenogranite.

Strontium is generally replacing Ca in the Ca-bearing minerals such as calcic amphibole and calcic plagioclases. These minerals are more dominant in the monzogranite than in the syenogranite. Also Cu and Cr concentrations are higher in monzogranite than in the syenogranite which may be related to their relatively high contents the magma of syenogranite as a result of magmatic contamination from migmatite country rocks existing to the east of the study the area.

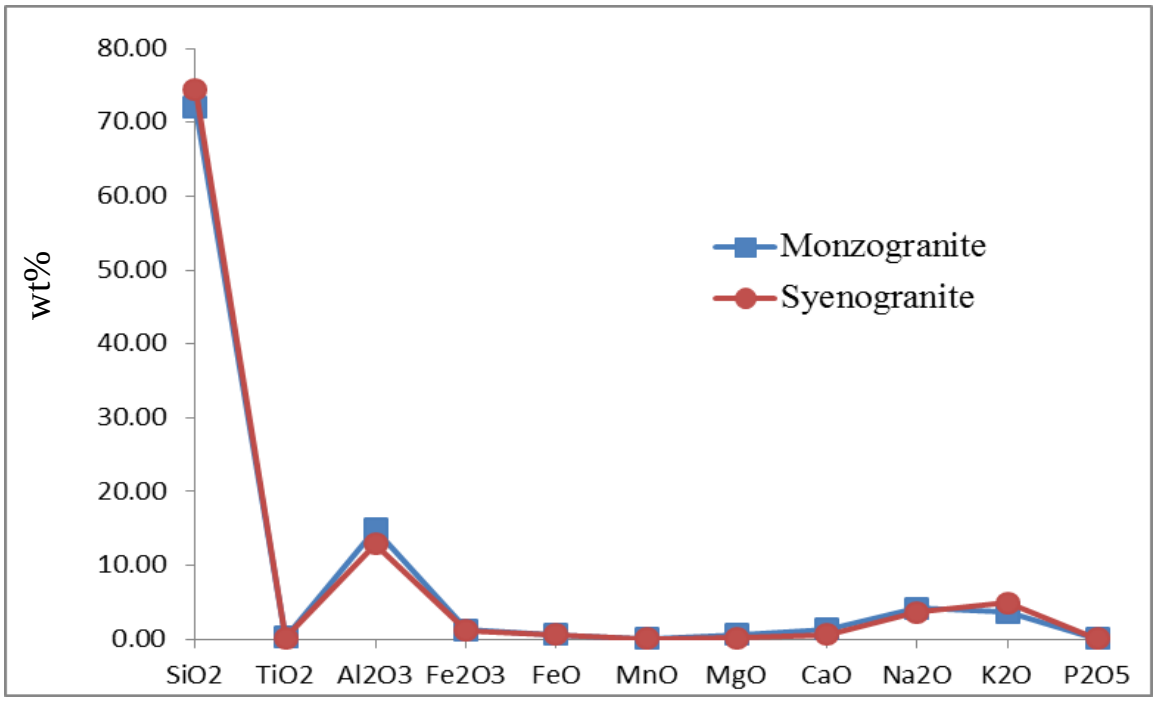

Fig. (4): Comparison between the average concentrations of the major oxides in the two granite types.

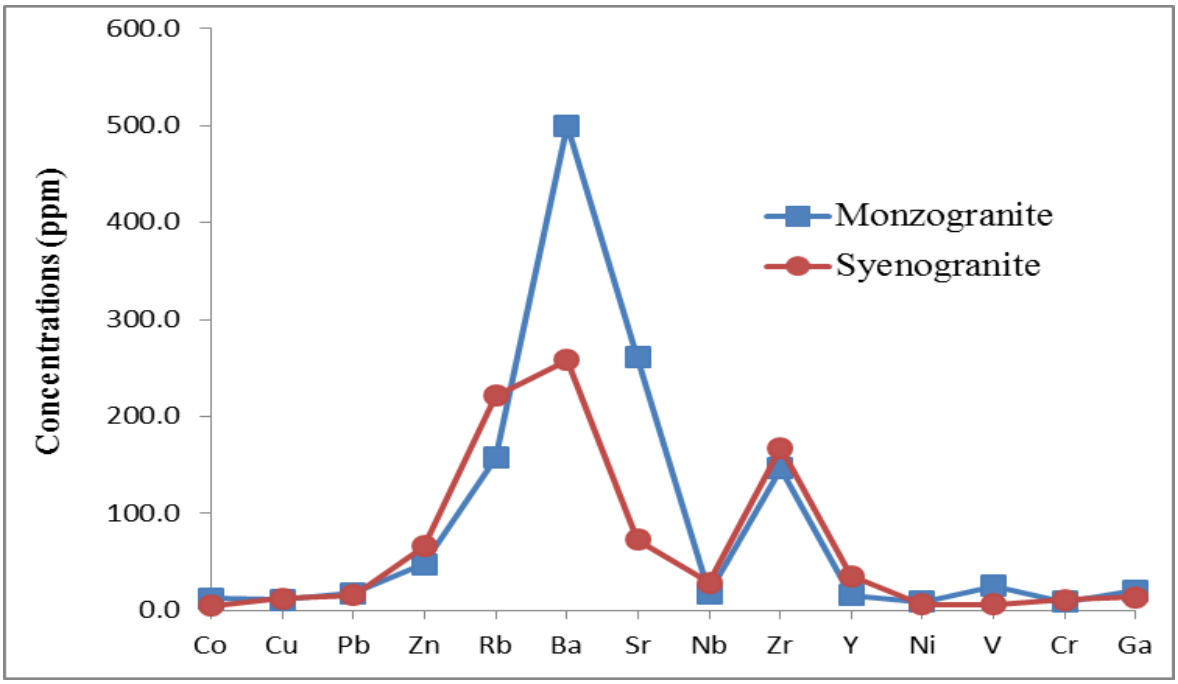

Fig. (5): Comparison between the average concentrations of the trace elements in the two granite types.

Table (1): The chemical analysis data and C.I.P.W. norm values for the studied monzogranite.

Sample No. / Major oxides (wt%)	M1	M2	M3	M4	M5	M6	M7	M8	Average
SiO_2	72.73	71.4	73.81	71.93	70.95	71.62	72.6	71.96	72.13
TiO_2	0.29	0.32	0.23	0.21	0.31	0.45	0.31	0.35	0.31
Al_2O_3	14.36	15.92	14.52	15.97	15.43	14.21	14.13	14.81	14.92
Fe_2O_3	0.86	1.35	0.97	1.65	1.19	1.95	0.99	1.11	1.26
FeO	0.81	0.83	0.68	0.46	0.61	0.72	0.76	0.18	0.63
MnO	0.03	0.08	0.03	0.04	0.07	0.06	0.05	0.08	0.06
MgO	0.81	0.73	0.17	0.51	0.49	0.75	0.71	0.92	0.64
CaO	1.51	1.26	1.12	0.93	2.15	1.46	1.37	0.97	1.35
Na_2O	3.41	4.15	4.01	3.37	4.02	4.1	3.21	4.23	3.81
K_2O	3.69	4.32	4.16	3.69	3.17	3.46	3.74	3.12	3.67
P_2O_5	0.1	0.11	0.05	0.05	0.12	0.15	0.06	0.13	0.10
L.O.I	0.82	0.3	0.23	0.72	0.74	0.94	0.51	1.13	0.67
Total	99.42	100.77	99.98	99.53	99.25	99.87	98.44	98.99	99.53
CIPW Norm									
Q	32.75	24.57	31.41	33.18	27.44	29.73	32.9	29.73	30.21
Or	22.06	25.33	24.65	21.99	18.93	20.65	22.46	18.76	21.85
Ab	32.12	38.29	34.88	32.61	39.08	36.75	32.44	40.9	35.88
An	6.98	5.56	5.27	4.36	10.06	6.42	6.55	4.12	6.17
C	1.65	1.64	1.3	4.11	0.81	1.04	1.51	2.14	1.78
Hy-en	2.05	1.81	0.43	1.28	1.24	1.89	1.8	2.34	1.61
Hy-fs	0.37	0.05	0.14	0	0	0	0.17	0	0.09
Mt	1.23	1.9	1.37	1.01	1.31	1.22	1.44	0.86	1.29
He	0	0	0	0.94	0.28	1.1	0	0.52	0.36
iL	0.56	0.6	0.44	0.4	0.59	0.86	0.6	0	0.51
AP	0.23	0.25	0.11	0.11	0.26	0.33	0.13	0.29	0.21
Total	100	100	100	99.99	100	99.99	100	99.66	99.96
Trace elements (ppm)									
Co	10	16	13	12	13	8	14	16	12.8
Cu	12	9	8	7	14	9	20	10	11.1
Pb	20	21	17	9	17	18	20	20	17.8
Zn	40	73	42	61	42	35	56	33	47.8
Rb	187	163	151	187	127	120	163	163	157.6
Ba	627	528	133	518	539	768	518	368	499.9
Sr	338	249	72	219	298	457	237	217	260.9
Nb	18	19	23	18	18	10	19	19	18.0
Zr	121	167	138	123	146	152	162	163	146.5
Y	12	16	16	12	21	15	21	14	15.9
Ni	13	9	8	9	9	11	7	8	9.3
V	38	40	25	28	11	7	32	23	25.5
Cr	10	7	8	8	8	20	7	6	9.3
Ga	21	22	25	21	20	20	17	21	20.9

Q=quartz, Or=orthoclase, Ab=albite, An=anorthite, C=corundum, Hy-en=hypersthene-enstatite, Hy-fs=hyperthene-ferrosilite, Mt=magnetite, He=hematite, il=ilmenite, Ap=apatite.

Table (2): The chemical analysis data and C.I.P.W. norm values for the studied syenogranite.

Sample No. / Major oxides (wt%)	S1	S2	S3	S4	S5	S6	S7	S8	Average
SiO_2	74.94	74.4	74.55	74.63	74.21	74.41	74.99	73.94	74.51
TiO_2	0.13	0.14	0.21	0.17	0.19	0.12	0.16	0.23	0.17
Al_2O_3	12.71	12.25	13.26	12.98	13.1	12.96	12.91	13.31	12.94
Fe_2O_3	1.25	1.35	0.99	1.86	1.25	0.91	1.12	1.14	1.23
FeO	0.57	0.96	0.42	0.71	0.53	0.99	0.64	0.57	0.67
MnO	0.04	0.05	0.05	0.04	0.07	0.03	0.06	0.03	0.05
MgO	0.17	0.13	0.3	0.25	0.22	0.16	0.21	0.13	0.20
CaO	0.62	0.51	0.81	0.56	0.66	0.73	0.75	0.62	0.66
Na_2O	3.96	3.82	3.97	4.32	3.71	3.96	3.88	3.86	3.94
K_2O	4.55	5.11	4.87	4.36	4.97	5.61	4.96	5.11	4.94
P_2O_5	0.03	0.07	0.29	0.05	0.04	0.12	0.05	0.04	0.09
L.O.I	0.61	0.96	0.16	0.11	0.96	0.37	0.79	0.42	0.55
Total	99.58	99.75	99.88	100.04	99.91	100.37	100.52	99.4	99.93
CIPW Norm									
Q	36.07	36.57	32.9	32.04	34.31	31.07	35.13	30.85	33.62
Or	26.46	30.29	28.95	25.83	29.53	33.35	29.32	30.54	29.28
Ab	31.95	27.27	31.77	35.73	29.8	29.39	28.8	32.96	30.96
An	2.92	2.13	2.33	2.49	3.06	2.93	3.43	2.87	2.77
C	0.63	0.53	0.98	0.39	0.82	0.11	0.66	0.38	0.56
Hy-en	0.43	0.33	0.75	0.63	0.55	0.4	0.52	0.33	0.49
Hy-fs	0	0.51	0	0	0	0.93	0.1	0	0.19
Mt	0.89	1.96	0.91	1.93	1.39	1.33	1.62	1.28	1.41
He	0.34	0	0.37	0.53	0.09	0	0	0.27	0.20
iL	0.25	0.27	0.4	0.32	0.36	0.23	0.3	0.44	0.32
Ap	0.06	0.14	0.64	0.11	0.09	0.26	0.11	0.09	0.19
Total	100	100	100	100	100	100	99.99	100.01	100
Trace elements (ppm)									
Co	3	4	5	3	5	8	6	3	4.6
Cu	10	4	9	2	7	52	5	12	12.6
Pb	3	6	7	9	21	28	30	25	16.1
Zn	51	76	59	32	131	40	59	80	66.0
Rb	96	259	241	298	244	207	209	215	221.1
Ba	178	246	304	293	220	302	216	306	258.1
Sr	59	61	90	81	67	78	63	87	73.3
Nb	23	33	26	34	32	34	30	20	29.0
Zr	118	137	175	195	183	186	176	169	167.4
Y	14	27	34	60	39	46	38	27	35.6
Ni	4	6	3	5	5	7	13	6	6.1
V	2	5	8	6	9	3	13	7	6.6
Cr	21	6	13	6	5	4	28	4	10.9
Ga	12	10	19	15	8	16	14	18	14.5

Q=quartz, Or=orthoclase, Ab=albite, An=anorthite, C=corundum,
Hy-en=hypersthene-enstatite, Hy-fs=hyperthene-ferrosilite, Mt=magnetite, He=hematite, il=ilmenite, Ap=apatite.

Applying the Qz vs. ANOR norms diagram shows that the data points plot in the monzogranite and syenogranite fields (**Fig. 6**). On the other hand, applying the AFM ternary diagram proposed by Irvine and Baragar [17] (**Fig. 7**) reveals that the data points of the studied granites plot into the calc-alkaline field; whereas, the syenogranite samples plot closer to the alkalie corner. Also, the use of the AFM ternary diagram which discriminates between the extensional and compressional regime [18] reveals that the syenogranite samples plot parallel to the A-F side signifying low MgO contents. This reflects emplacement within an extensional (anorogenic) regime, whereas those of the monzogranite seem to be of compressional environment.

On the other hand, applying the Ba–Rb–Sr ternary diagram of El Gaby [19] revealed that the monzogranite data points fall into the field of anomalous granite and close to the line of contact with the granodiorite field (**Fig. 8**). The syenogranite samples plot within the field of strongly differentiated granite which indicates a very late differentiation stage enriched in Rb.

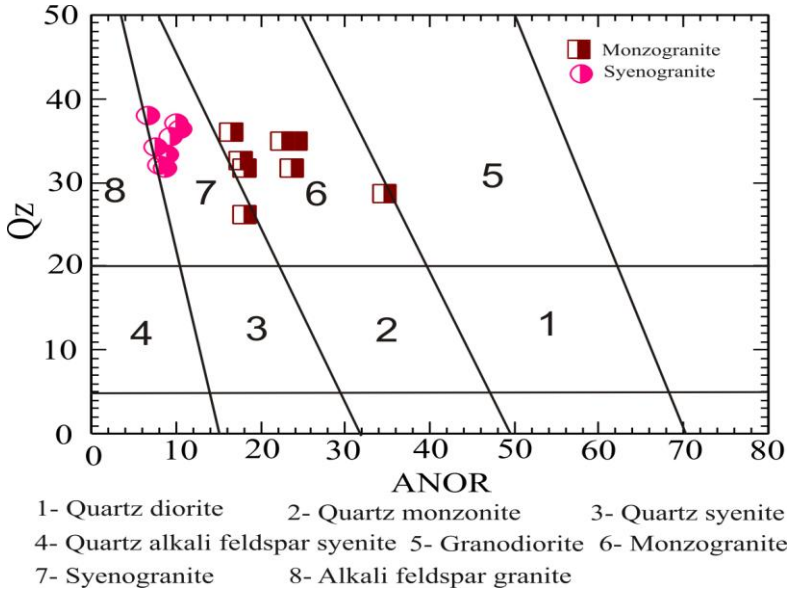

Fig. (6): Plot of the studied granites on the ANOR- Qz diagram, proposed by Streckeisen and LeMaitre [20].

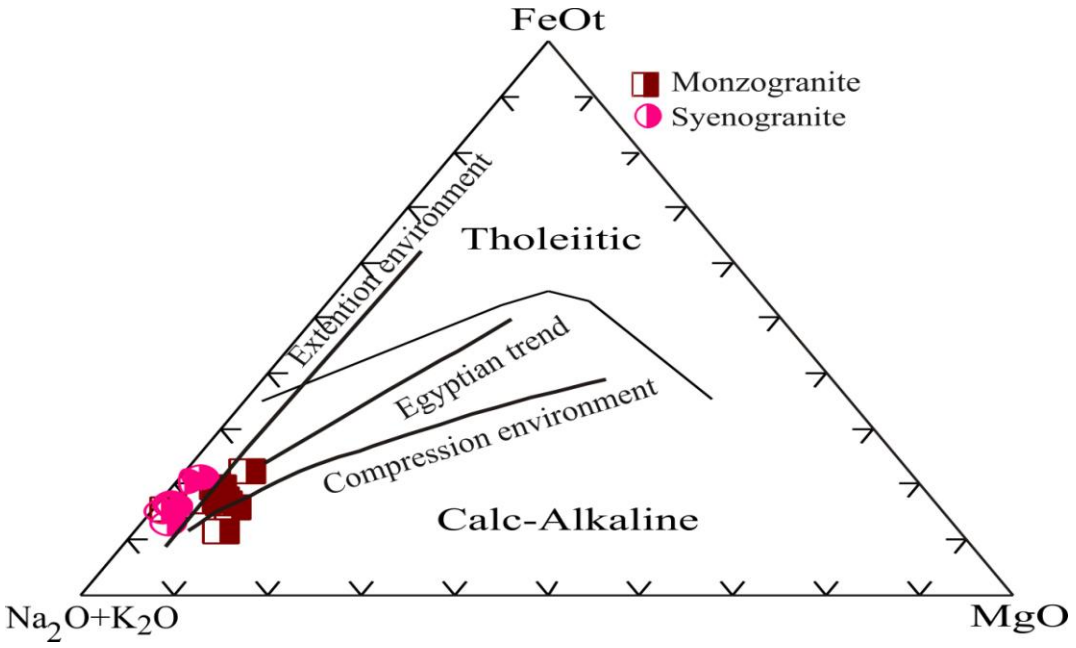

Fig. (7): Plot of the studied granite on the AFM ternary diagram adopted by Irvine and Baragar [17]. The trends of compressional and extensional suites are proposed by Petro et al. [18]. The trend of Egyptian granites is defined after Hussein et al. [21].

The nature of magma from which the studied granites were derived could be determined by plotting their data points on the A/CNK-A/NK diagram of Maniar and Piccoli [22]. **Figure (9)** shows that the monzogranite was derived from peraluminous magma whereas the syenogranite was crystalized from a magma having characters which are transitional between peraluminous and metaluminous. This was confirmed by examining the CIPW normative mineralogy (**Tables 1 and 2**). The monzogranite samples have values of normative corundum ranging from 0.81 to 4.11 which is compatible with the peraluminous affinity suite whereas those of the syenogranite samples range from 0.11 to 0.98 which are compatible with the moderately-transition zone between peraluminous and metaluminous affinity suites.

Batchelor and Bowden [23] used the R1-R2 diagram proposed by De La Roche et al. [24] to discriminate between the tectono-magmatic environments during the orogenic cycles of granitic magma generation. Plotting the studied samples on this diagram (**Fig. 10**) shows that the monzogranite fall into the late-orogenic field whereas these of the syenogranite plot in the anorogenic field. This suggests an extensional regime of emplacement.

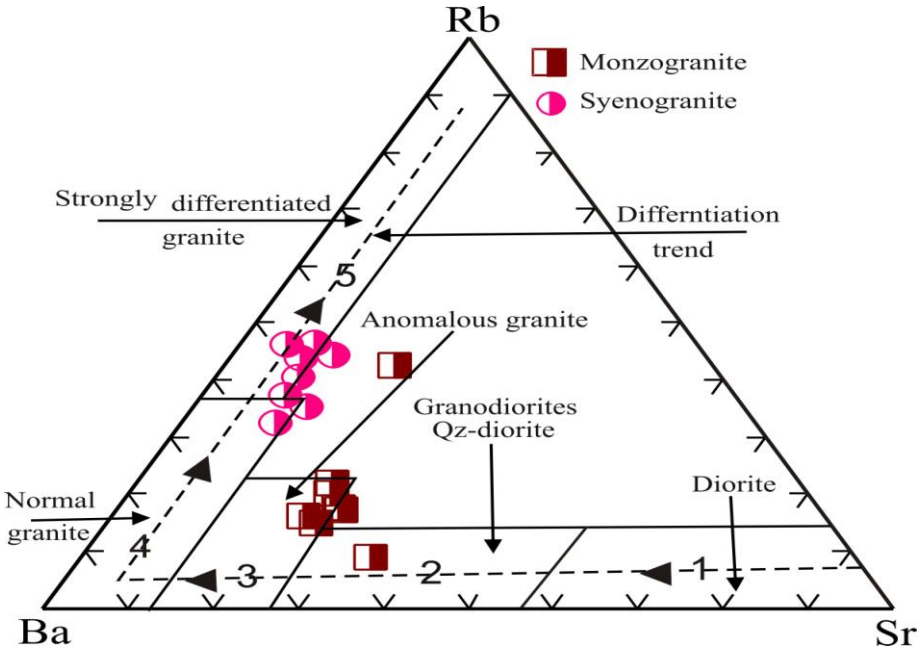

Fig. (8): Plot of the studied granites on the Ba-Rb-Sr diagram proposed by El Bouseily and El Sokkary [25].

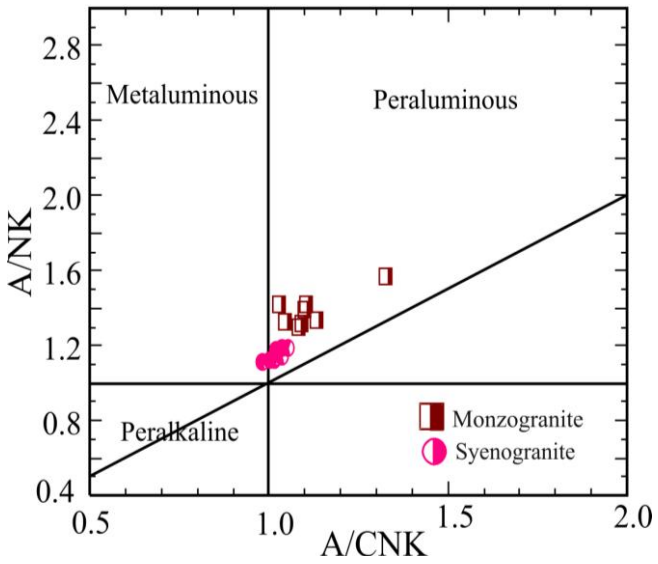

Fig. (9): Plot of the studied granites on the A/CNK-A/NK diagram proposed by Maniar and Piccoli [22].

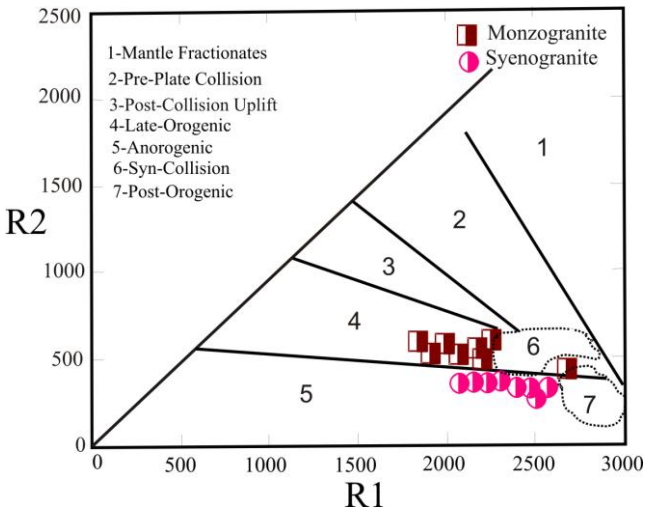

Fig. (10): Plot of the studied granites on the R1-R2 diagram proposed by De La Roche et al. [24]. The tectonic setting fields are given by Batchelor and Bowden [23].

To discriminate between the A-type granite and the M, S, I types, Whalen et al. [26] used of the variation of Y versus 10000*Ga/Al. Applying this diagram (**Fig.11**) shows that the syenogranite samples plot in the A-type field whereas those of the monzogranite fall into the M, S, I types field. Anorogenic magmatism, which produces A-type granitic rocks, is typically associated with the post-orogenic and/or intracontinental rift settings. It is especially common in the Mesoproterozoic and is linked to the emplacement of high-heat producing granites (HHP), which may host world-class U and REE ore systems including Fe oxides-gold-copper deposits (such as the Olympic Dam in south Australia). In addition, the emplacement of HHP results in the inception of a large-scale hydrothermal activity [27].

The tectonic environment in which the granitic rocks were evolved was discussed by Pearce et al. [28]. They used the variation of Rb vs. Nb+Y. Applying this relationship (**Fig. 12**) shows that the monzogranite samples fall into the volcanic-arc field while those of the syenogranite plot in the within-plate granite field.

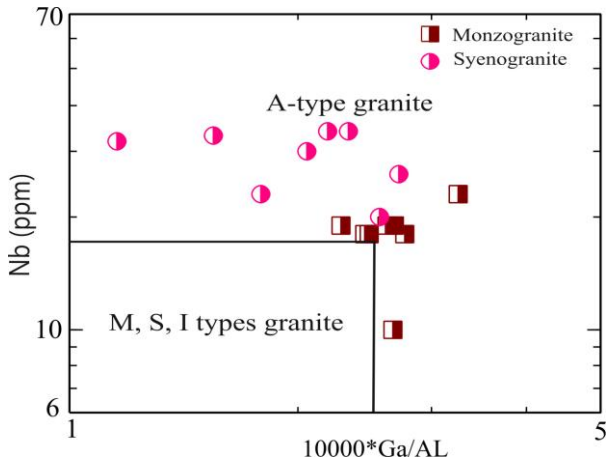

Fig. (11): Plot of the studied rocks on the 10000*Ga/Al vs. K_2O+Na_2O, Y, Zr and Nb discrimination diagram adopted by Whalen et al. [26].

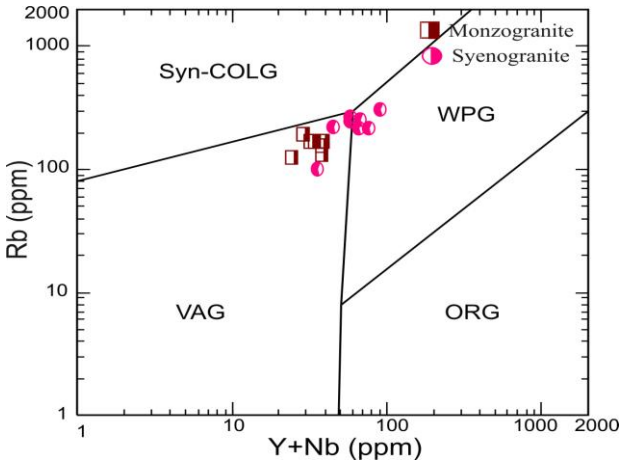

Fig. (12): Plot of the studied granites on the Rb-(Y+Nb) tectonic discrimination diagram proposed by Pearce et al. [28].

In conclusion, the studied syenogranite is relatively enriched in Rb, Y and Nb similar to most of the within-plate granites. This can be explained in terms of derivation from a mantle source enriched in incompatible elements [29], or significant crustal involvement. On the other hand, the studied monzogranite displays several features characteristic of the I-type granites which originated from peraluminous magma that was emplaced in volcanic-arc tectonic environment. It was mostly derived from mantle and later modified by subduction components and selective enrichment in incompatible elements. The syenogranite is considered as A-type granite that was derived from a magmatic suite having composition at a moderately transition zone between the peraluminous and metaluminous affinities. It was crystallized at the within-plate tectonic regime.

2- Spectrometry

The Wadi Akhdar anomaly is localized along the shear zone trending NW-SE and situated at the contact between the monzogranite and the syenogranite along a dip-slip fault. This zone is traversed by a number of pegmatitic dykes and pockets as well as quartz veins.

The data obtained from the detailed surface ground spectrometric survey which was conducted on the anom alous zone and on the its border from monzogranite and syenogranite are given in **table (3)** and displayed as spectrometric contour maps in latitude-longitude UTM WGS 84 and also in the degree, minutes and second system. These data revealed the following:

2.a- The equivalent uranium (eU) spectrometric levels

The equivalent uranium (eU) spectrometric contour map (**Fig. 13**) shows that its concentration ranges between 2.4 ppm and 1100.4 ppm with an average of 70.65 ppm (**Table 3**). The eU map shows that the high concentrations extend in the same NW-SE trend of the shear zone.

2.b- The equivalent thorium (eTh) spectrometric levels

The equivalent thorium (eTh) intensity ranges between 9.7 ppm and 644.7 ppm with an average of 59.71 ppm (**Table 3**). The spectrometric contour map (**Fig. 14**) shows that the high concentrations of equivalent thorium (eTh) follow the same high radioactive NE-SW trend.

2.c- eU/eTh ratio spectrometric levels

The eU/eTh ratio is generally used to determine any secondary processes of uranium enrichment and/or depletion. If this Ratio highest than 1/3 indicate uranium enrichment. The calculated eU/eTh ratios of Wadi Akhdar shear zone range from 0.06 to 17.52 which indicates uranium enrichment.

The spectrometric contour map of the eU/eTh ratios (**Fig. 15**) displays one dominant trend which can be definitely correlated with that obtained for the eU. This indicates that eU progressively increases with the increase in the eU/eTh ratio along the anomalous zone. This result is consistent with that obtained by Charbonneau and Ford [30] who emphasized that an increase in equivalent uranium along with the increase in eU/eTh ratio may suggest a zone of uranium mineralization.

2.d- The eTh/eU ratio spectrometric levels

The wide variations in the calculated eTh/eU ratios in the studied shear zone (**Table 3**) signify variation in uranium concentration.Consequently, this variation could be attributed to differences in the equilibrium and disequilibrium ststes from place to place. This reflects variations in conditions of precipitation as well as leaching-enrichment at different places within shear zone. These variations could be related to some factors which controlled the hydrothermal solution precipitation processes. These factors comprise changes in chemical reactions, temperature, pressure, pH and Eh. The eTh/eU spectrometric contour map (**Fig. 16**) reveals the presence of relatively high eTh concentrations in the NE-SE trend.

In conclusions, the total radioactivity of shear zone anomalous zone is mainly attributed to the presence of uranium and thorium minerals. This is confirmed by the concordance of the radioactive NW-SE trend on the previously mentioned eU, eU/eTh and eU/eTh spectrometric contour maps.

Table (3): Ranges and averages of eU, eTh (ppm) concentrations and eU/eTh and eTh/eU ratios of the studied shear zone and its contacted part of syeno-and monzogranites.

Statin No. 67	eU (ppm)	eTh (ppm)	eU/eTh ratio	eTh/eU ratio
Minimum	2.4	9.7	0.06	0.06
Maximum	1100.4	644.7	17.52	16.21
Average	70.65	59.71	0.65	5.52

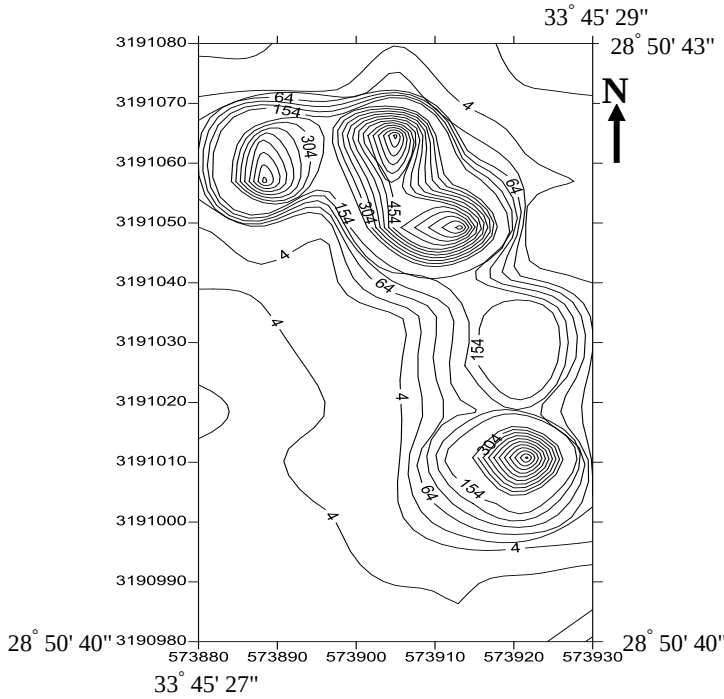

Fig. (13): Spectrometric contour map for the equivalent uranium (eU) of the anomalous shear zone, Wadi Akhdar

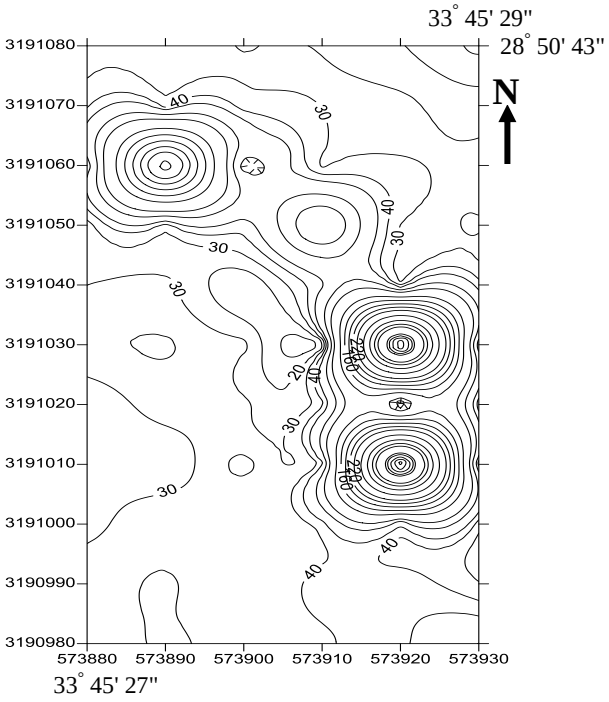

Fig. (14): Spectrometric contour map for the equivalent thorium (eTh) of the anomalous shear zone, Wadi Akhdar area.

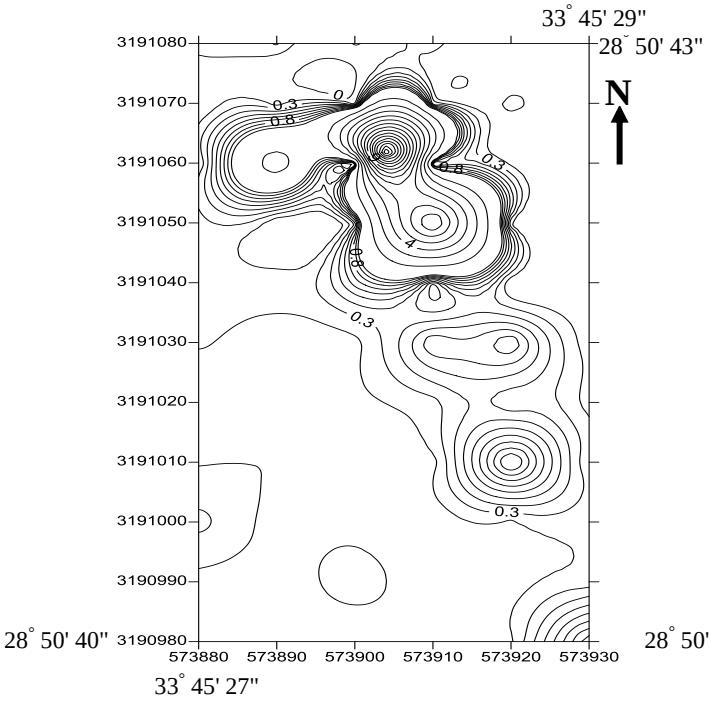

Fig. (15): Spectrometric contour map for the eU/eTh ratio of the anomalous shear zone, Wadi Akhdar area.

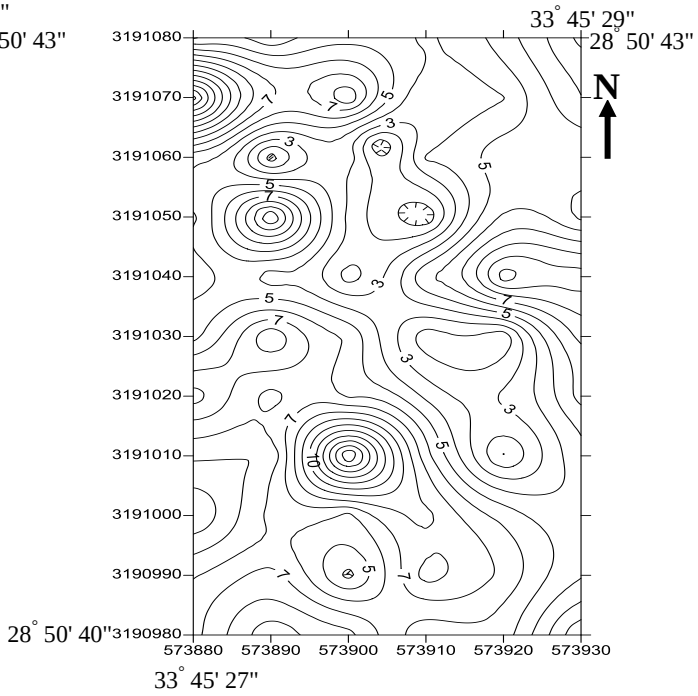

Fig. (16): Spectrometric contour map for the eTh/eUh ratio of the anomalous shear zone, Wadi Akhdar area.

3- Mineralogy

The mineralogic examination of studied shear zone revealed that the rocks contain a mineral association consisting of uraninite, uranpyrochlore, davidite-(Ce) liandratite walpurgite, thorogummite and weeksite. These minerals are reported for the first time in the studied shear zone.

3.a- Uraninite (UO_2)

Uraninite is a common accessory mineral in pegmatites and peraluminous granites and is the most important source of dissolved uranium in groundwater emanating from weathered granite terrains [31]. Uraninite was identified in samples from the quartz veins and pegmatite pockets and dykes within the shear zone. It is a reduced mineral and found associated with other actinide and non-actinide elements. The occurrence of uraninite in mineralized zone is usually considered as evidence for primary deposits. Nash et al. [32] stated that, in passing of uranium from its hexavalent state to the tetravalent state (oxidizing to reducing conditions) and in the presence of redacting agent metal ions, such as Na^+, K^+, Ca^{2+}, Cu^{2+} and Fe^{2+}, the solubility of the uranyl complexes decreases and very complex U salts are precipitated. Pirajno [27] describe the relationship of uraninite with hematite as, it is not clear, but it is possible that the oxidation of Fe causes the reduction of U from its $^+6$ to $^+4$ state, facilitating its precipitation according to:

$$3H_2O+Fe^{2+}+(U^{6+}O_2)^{2+} \longrightarrow Fe_2O_3+6H^+ +U^{4+}O_2 \text{ (uraninite)}$$

The detected uraninite exists in two forms, the first is represented by euhedral to subhedral cubic crystals (**Fig. 17 A**) disseminated within pegmatitic and quartz pockets. The second form consists of minute inclusions and/or substitutionary overgrowths with uranpyrochlore crystals that are disseminated within the hydrothermal veins as well as the walls of altered granite. It shows a wide range of colors from the usual brownish black variety with typical conchoidal fracture to the greyish black and black variety. Uraninite is associated with uranpyrochlore, davidite-(Ce), liandratite, walpurgite, thorogummite and weeksite grains. This association may indicate formation by hydrothermal fluids [33]. **Figures 17 C & D** show the X-ray-diffraction pattern and the ESEM analyses supported by EDAX for the detected uraninite. The strongest three lines in the X-ray diffraction pattern of the recorded uraninite have (d) values equal to 3.157 Å, 1.93 Å, 1.64 Å. Its EDAX data confirm the characterization of uraninte. It is composed of UO_2 (42.74%), Nb_2O_5 (28.12%), Fe_2O_3 (7.20%), TiO_2 (8.43%), SiO_2 (5.52%) and CaO (4.87%). Al_2O_3 and TaO exist in minor concentrations (2.76% and 0.36%, respectively). Frondel [34] described two types of uraninite; magmatic and hydrothermal. Magmatic uraninites commonly have $ThO_2 \geq 2\%$ while the hydrothermal variety has zero to 0.25% of ThO_2. The obtained chemical analysis data reveal that ThO_2 is under the detection limit, suggesting a hydrothermal origin for the detected uraninite.

3.b- Uranpyrochlore [(U,Ca, Ce)$_2$(Nb, Ta)$_2$O$_6$(OH, F)]

Uranpyrochlore is a uranium-dominant end-member of pyrochlore. It was recorded in the pegmatite occurring as black, yellowish brown, subhedral crystals showing a substitutionary overgrowth with uraninite (**Fig. 17 B**). It has XRD spacings at 3.01 Å, 1.84 Å and 2.61 Å (**Fig. 17 C**).

The EDAX data (**Fig. 17 E**) reveals the characteristics of uranpyrochlore minera. It indicates the presence of high concentrations of titanium (37.81%), uranium (20.57%), niobium (16.39%), iron (13.06%) and silica (7.87%). Minor proportions of alumina (2.84%), calcium (1.12%) and manganese (0.34%) are present.

3.c- Davidite-(Ce) [(Ce, La) (Y,U, Fe^{2+}) (Ti,Fe^{3+})$_{20}$ (O,OH)$_{38}$]

Davidite was recorded in hydrothermal veins and on the walls of the granitic country rocks which confirm its hydrothermal origin. It is represented by dark brown to black, subhedral to anhedral crystals having a glassy to submetallic luster and moderate hardness (**Fig. 18 A**). It exists in irregular forms coleform or botryoidal masses. The XRD and ESEM examinations of the picked grains show that davidite associated with liandratite and walpurgite. The X-ray diffraction peaks of davidite occur at 1.69, 1.7 and 1.43 Å (**Fig. 18 C**). Its EDAX data confirm the characterization of davidite and liandratite minerals (**Figs. 18 D and E**).

3.d- Liandratite [U^{6+}(Nb, Ta)$_2$O]

Liandratite was detected in hydrothermal veins and on the walls of fractures which acted as pathways for solutions. It occurs as grains, crusts or coatings of davidite crystals. Its color is yellow to brown while the streak is bright yellow (**Fig. 18 B**). The association of the uranium-bearing niobotantalate (uranpyrochlore and liandratite) with uranium minerals (uraninite, davidite and thorogummite) indicates the enrichment of the hydrothermal solutions in niobium, tantalum and iron. The presence of davidite inclusion within liandratite crystals strongly suggests that the mineral was crystallized much later than davidite. The X-ray diffractograms and ESEM patterns of liandratite are shown in Figures **18 C and E**.

3.e- Walpurgite [Bi$_4$(UO$_2$)O$_4$(AsO$_4$)$_2$. 2H$_2$O]

Walpurgite is a rare secondary mineral of a hydrated bismuth uranyl arsenate oxide. It was recorded as coatings of some davidite and liandratite crystals. They have straw yellow color crystals, translucent to transparent and existing in the hydrothermal veins and their walls in the younger granites. The obtained XRD pattern of walpurgite is shown in **Figure 18 C**.

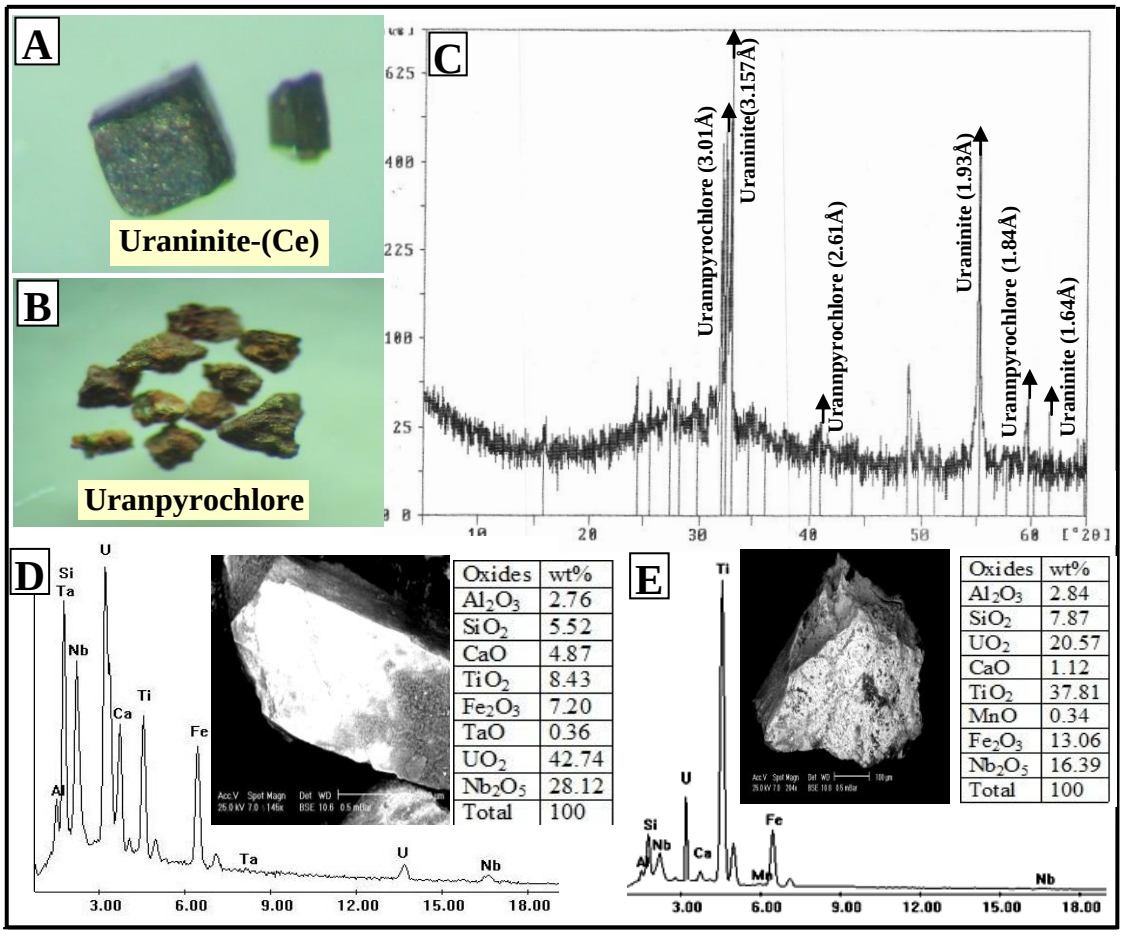

Fig. (17): (A) & (B) Photomicrographs (x64) of uraninite and uranpyrochlore crystals respectively, **(C)** XRD pattern of the two minerals, **(D)** and **(E)** BSE images, and EDAX charts show the characterization of the of these minerals.

3.f- Thorogummite [$(Th,U^{6+})(SiO_4)_{1-x}(OH)_{4x}$]

Thorogummite differs from thorite in being secondary in origin and formed by the alteration of primary thorium minerals including thorite and thorianite. It was recorded within the pegmatitic dykes and pockets as crystalline fine-grained aggregates having yellowish brown to black color and subvitreous luster (**Fig. 19 A**). Its X-ray-diffraction and ESEM pattern are showen in **Figures 19 C and D**. The composition of thorogummite is dominated by ThO_2 (60.97%), SiO_2 (16.22%) and UO_2 (12.34%). In addition, Y_2O_3, CaO, Fe_2O_3, SO_3 and Ce_2O_3 exist in lesser concentration. While Pr_2O_3 is a minor constituent (0.45%).

3.g- Weeksite [$K_2 (UO_2)_2 Si_6O_{15} . 4H_2O$]

Weeksite was recorded in the hydrothermal veins and their walls. It exist in the form of radiating and fibrous aggregates and encrustations intergrowths with the quartz having yellow color and waxy to silky luster **Fig. 19 B**. The X-ray pattern indicates its presence in association with thorogummite **(Fig. 19 C)**. It is characterized by three major X-ray diffraction peaks at 7.11, 3.30 and 3.20 Å. The characteristics of the chemical composition of the reported weeksite are given in **Figure 19 E**. The high content of Th in the weeksite chemical data analysis due to thorogummite association.

Discussion

The younger granites of Wadi Akhdar area are differentiated to monzogranite and syenogranite. The monzogranite has peraluminous characters indicating a late orogenic, volcanic-arc tectonic setting. It is classified genetically as I-type granite. Syenogranite, on the other hand, has a composition which falls in moderately transition zone between peraluminous and metaluminous affinity. It indicates an anorogenic, within-plate tectonic setting and is classified as A-type granite.

In this study, the spectrometric and the mineralogical examinations studies carried out on the shear zone reveal the presence of high uranium and thorium concentrations, some the uranium minerals contain rare metals. They exist as fracture-fillings, swarms of pegmatitic pockets and dykes and quartz veins. These minerals have hydrothermal origin.

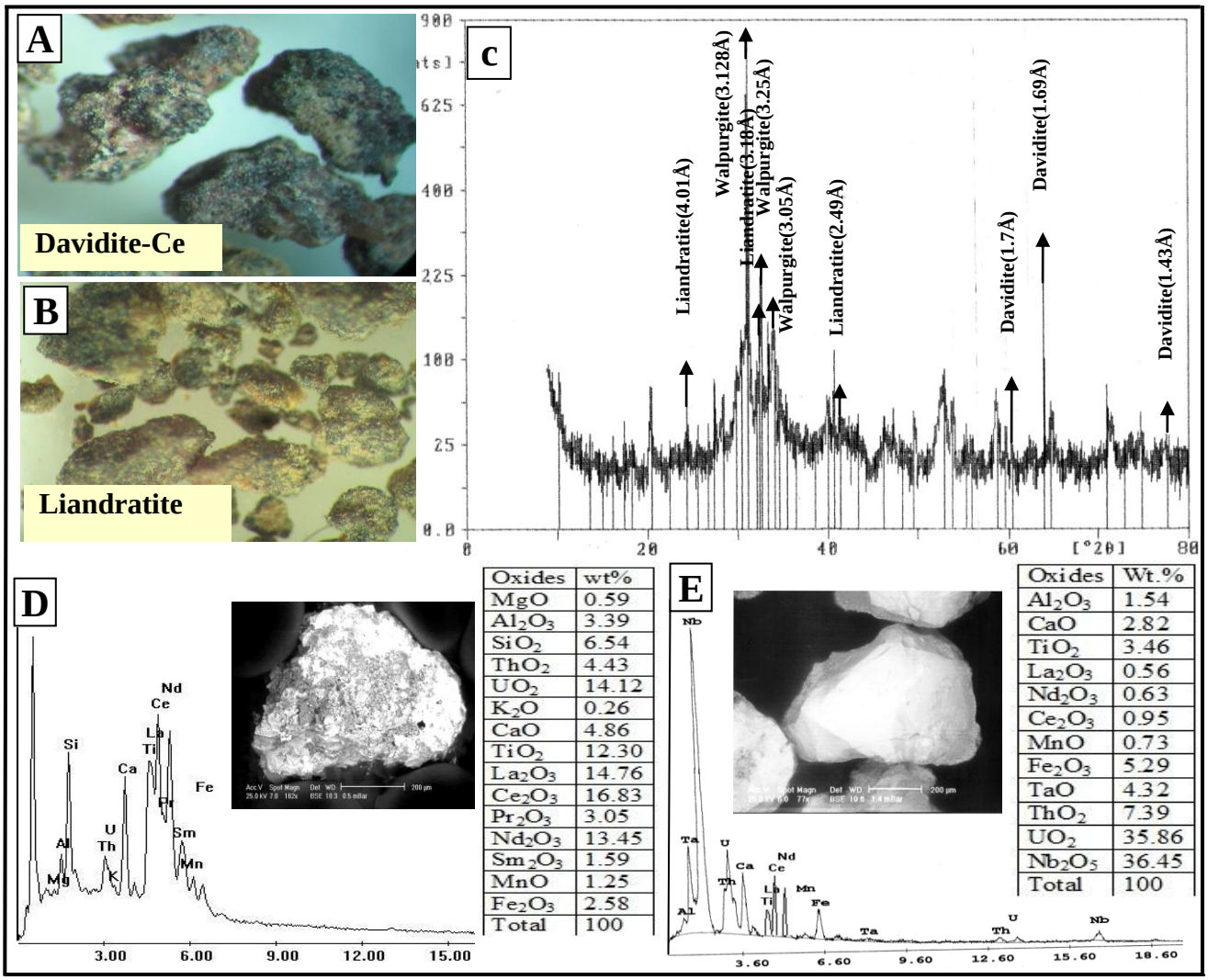

Oxides	wt%
MgO	0.59
Al_2O_3	3.39
SiO_2	6.54
ThO_2	4.43
UO_2	14.12
K_2O	0.26
CaO	4.86
TiO_2	12.30
La_2O_3	14.76
Ce_2O_3	16.83
Pr_2O_3	3.05
Nd_2O_3	13.45
Sm_2O_3	1.59
MnO	1.25
Fe_2O_3	2.58
Total	100

Oxides	Wt.%
Al_2O_3	1.54
CaO	2.82
TiO_2	3.46
La_2O_3	0.56
Nd_2O_3	0.63
Ce_2O_3	0.95
MnO	0.73
Fe_2O_3	5.29
TaO	4.32
ThO_2	7.39
UO_2	35.86
Nb_2O_5	36.45
Total	100

Fig.(18): (A) & (B) Photomicrographs (x64) of davidite-Ce and liandratite crystals respectively, **(C)** XRD pattern of the davidite-Ce, liandratite and walpurgite minerals, **(D)** and **(E)** BSE images and EDAX charts of the davidite-Ce and liandratite minerals respectively.

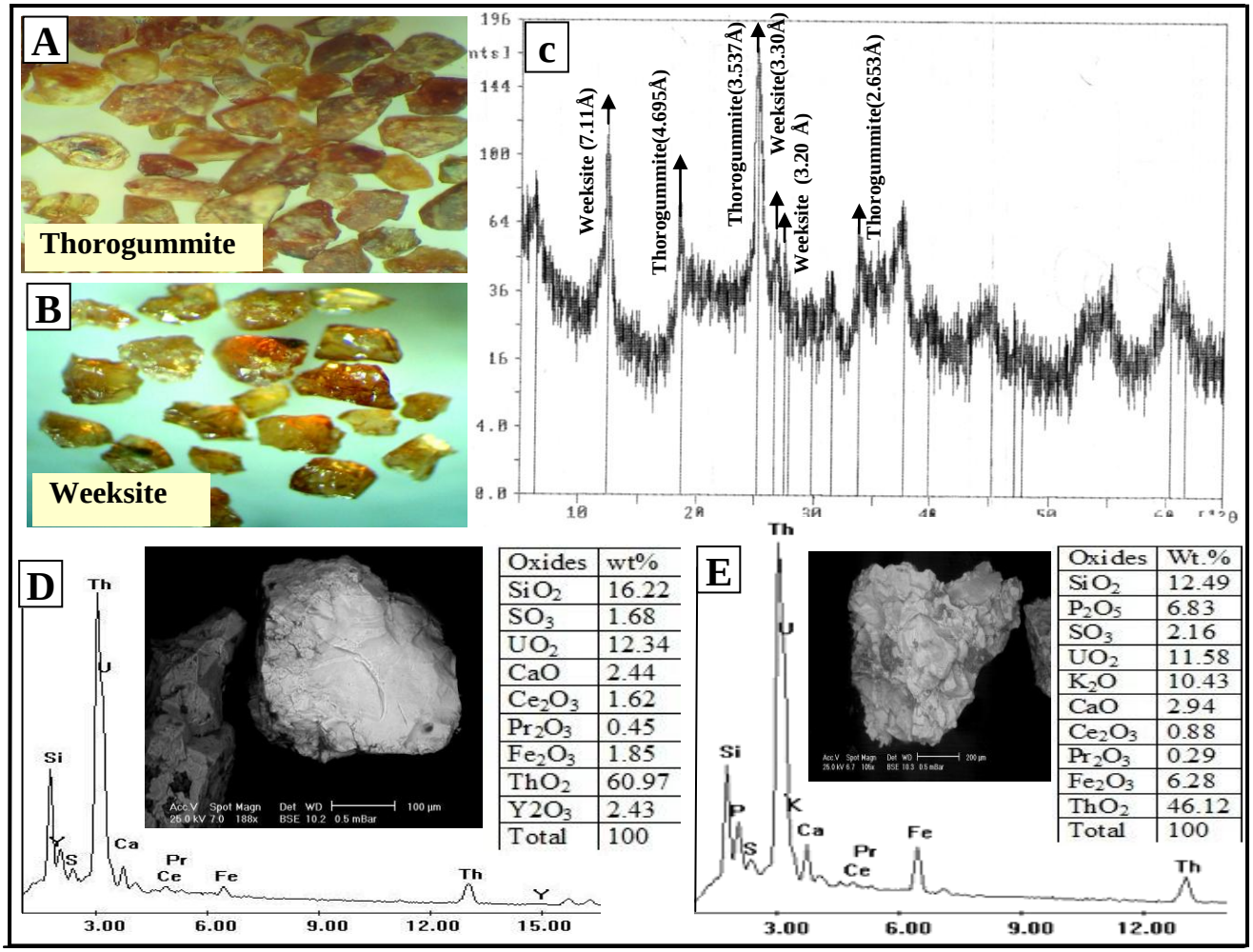

Fig.(19): (A) & (B) Photomicrographs (x64) of Thorogummite and Weeksite crystals respectively, **(C)** XRD pattern of the two minerals, **(D)** and **(E)** BSE images and EDAX charts of these minerals.

Evidently, the study area was affected by successive hydrothermal events which occurred during all the orogenic stages of convergent, collision to post-collision tectonics as well as emplacement of anorogenic granite intrusion. Also, the area witnessed hydrothermal activities that are related to various deformation events which included faulting, fracturing and development of dilation zones. These brittle deformations are generally related to a major, of structure regional-scale such as the Gulf of Suez, Gulf of Aqaba and Red Sea rifting. Pirajno (2010) stated that orogenic processes which favour large-scale generation and transportation of hydrothermal fluids are subduction-related systems and collision-related orogens. Fluids are generated during convergent processes which result in compression, deformation and prograde metamorphism of sedimentary wedges and subducted oceanic crust. Considering the above mentioned information, the study area represented a favorable environment for the accumulation of uranium and other hydrothermal-related deposits.

The results of mineralogical investigation of the study area revealed the presence of anomalous concentrations of metallic minerals which exist in one localized mineralized shear zone. This zone is dominated by fracture networks, swarms of pegmatitic pockets, quartz veins and pegmatitic and aplite dykes. They are scattered along the two sides of the contact between the two phases of younger granites. This zone is deformed and acted as a pathway for ascending and descending mineralizing solutions. The latter might have included meteoric and formation waters as well as fluids released during the thermal metamorphism which resulted from the intrusion of the granitic magma at open system in addition to fluids liberated during the magmatic processes. Generally, the hydrothermal veins (such as quartz and calcite veins) are good indicators of hydrothermal fluid flow and can also be considered as an expression of the conduits or fractures through which fluids circulated. Hydrothermal alteration is very important for mineral exploration because it extends well beyond the limits of the ore, hence, allowing the focusing of exploration activity towards smaller targets. Indeed, mapping of the alteration mineral assemblages can be very useful for the identification of hydrothermal conduits which, in turn, may lead to the discovery of buried ores. Uranium and associated metals may be derived locally in the rocks through which the mineralizing solutions migrate. In the studied mineralized zone, uranium occurs principally in

the quadrivalent state within its own primary mineral uraninite. Also, it exists as substitution and/or uranyl U^{6+} minerals associated with REE and some base metals and nonmetals such as Th, Si, K, Ca, Al, Fe, Ti, Mn, Nb, Ta, Y, Bi, As, S, and F. These assemblages reflect the higher content of cations in the mineralized solutions. Although the percentages of uranium- and rare metals- bearing minerals in the studied shear zone are low and insufficient to form economic ores however, their roles as marker minerals for "fertile U-source environments" feeding supergene and/or hypogene U deposits cannot be emphasized highly enough.

Conclusions

The Wadi Akhdar area is made up mainly of syenogranite, monzogranite and granodiorite. One shear zone exists in the two sides of the contact between the two phases of the younger granites. This shear zone is dissected by several mineralized pegmatitic dykes and pockets, swarms of hydrothermal veins and aplite dykes which induce difficulties in the mineralogical studies of this area.

The younger granites of Wadi Akhdar area have normal geochemical background. So, the magmatic origin of the mineralized zones can be excluded and, instead, the hydrothermal origin is much more probable. The studied monzogranite has many features characteristic of the I-type granites. It originated from peraluminous magma that was emplaced in a volcanic-arc tectonic environment. It was mostly derived from the mantle and later modified by subduction-related components and selective enrichment in incompatible elements. The syenogranite, on the other hand, is considered as A-type granite that was derived from a magmatic suite having composition at moderately transition zone between peraluminous and metaluminous affinity and was crystallized at the within-plate tectonic regime. Several uranium and rare metals-bearing minerals were recorded in the shear zone existing in the studied younger granites, They include uraninite, uranpyrochlore, davidite-(Ce), liandratite, walpurgite, thorogummite and weeksite; the latter is reported for the first time in the study area.

References

1) **El-Sheshtawy, Y. A. (1984).** Petrographical and geochemical studies of granitic rocks around Wadi El-Sheikh, southwestern Sinai, Egypt. Ph.D. Thesis, Al-Azhar univ., Cairo, Egypt, 185 p.
2) **El-Gammal, S. A. S. (1986).** Geology of the granitoid rocks of the northwestern part of the basement rocks in Sinai, Egypt. Ph.D. Thesis, Al-Azhar Univ., Cairo, Egypt, 255 p.
3) **Abu El-Enen, M. (1989).** Geology and geochemical studies of Wadi El-Seih area, southwest Sinai, Egypt. M.Sc. Thesis, Mansoura Univ., Mansoura 134 p.
4) **El-Metwally, A. A., Zalata, A. A. and Abu El-Enin M. M. (1992).** The evolution of the Pan-African granitoid rocks: Geochemical evidences from southwest Sinai massif, Egypt. J. Afr. Earth Sci., **14**(1): 111 – 119.
5) **Sherif, H. M. (1992).** Geology and radioactivity studies of Wadi El-Berra, south Sinai, Egypt. M. Sc. Thesis, Suez Canal Univ., Egypt, 129 p.
6) **Sherif, H. M. (1997).** Geology and uranium potentiality of Wadi Seih area, southwestern Sinai, Egypt. Ph. D. Thesis, Cairo Univ., Egypt, 229 p.
7) **Akaad, M. K., Noweir, A. M. and Kotb, H. (1979).** Geology and petrochemistry of the granite association of Arabian Desert Orogenic Belt between latitudes 25° 35` and 26° 30` N. Delta J. Sci., **3**: 107-151.
8) **Akaad, M. K. and Noweir, A. M. (1980).** Geology and lithostratigraphy of the Arabian Desert Orogenic Belt between latitudes 25° 35` and 26° 30` N. Symp. on "Evolution and Mineralization of Arabian and Nubian Shield". Inst. Appl. Geol. (Jeddah), Bull. **4**(3): 127-135.
9) **Rogers, J. W. and Greenberg, J. K. (1983).** Summary of recent work on Egyptian Younger Granites. J. Geol. Surv. Egypt, **XIII**: 185 – 191.
10) **Higazy, M., Abu El-Leil, I., Abdel Tawab, M. and El-Gammal, S. (1989).** Geological setting, structure and petrography of the granitic rocks in the north-western part of the basement rocks of Sinai, Egypt. Ann. Geol. Surv. Egypt, **XVI**: 149 – 157.
11) **Abdel-Karim, A. M. (1992).** Petrology of Late Precambrian younger granites from southwest Sinai. Proc. 3rd Conf. Geol. Sinai Develop, Ismailia, 267 – 272.
12) **Azzaz, S. A. (1993).** Petrogenesis of granitoid rocks of Wadi Baba area, southern Sinai, Egypt. JKAU: Earth Sci., **6**: 79 – 98.
13) **El-Tokhy, M. M. (1983).** Geology of Wadi El-Sheikh area, Sinai, Egypt. M.Sc. Thesis, Department of Geology, Mansoura Univ., 160 p.
14) **Ibrahim, M. E. A. (1991).** Geology and radioactivity of wadi-Zghra area, south central Sinai, Egypt. Ph.D. Thesis, Mansoura Univ., Egypt, 181p.
15) **Shapiro, L. and Brannock, W. W. (1962).** Radioanalysis of silicate, carbonate and phosphate rocks. U.S. G. S. Bull. 1114.
16) **El-Reedy, M. W. (1984).** The general physical and chemical features and the pollution level of El-Sabahia – Sabhan – El-Reqa soil localities, State of Kuwait. Internal Report Environment Protection Dept., Ministry of Pub. Health, El-Kuwait (Part. 1 : Chemical methods), 10p.
17) **Irvine, T. N. and Baragar, W. R. A. (1971).** A guide to the chemical classification of the common volcanic rocks. Can. J. Ear. Sci., **8**: 523-548.
18) **Petro, W. L., Vogel, T. A. and Wilband, J. T. (1979).** Major element chemistry of plutonic rock suites from compressional and extensional plate-boundaries. Chem. Geol., **26**: 217-235.

19) **El-Gaby, S. (1975).** Petrochemistry and geochemistry of some granites from Egypt. N. Jb.Minerl. Abh., **124**: 147-189.
20) **Streckeisen, A. L. and Le Maitre, R. W. (1979).** A chemical approximation to the modal QAPF classification of the igneous rocks. N. J.ahrb. Miner. Abh., **136**: 169-206.
21) **Hussein, A. A., Ali, M. M. and El-Ramly, M. F. (1982):** A proposed new classification of the granites of Egypt. J. Volc. Geoth. Res., **14**: 187-198.
22) **Maniar, P. D. and Piccoli, P. M. (1989).** Tectonic discrimination of granitoids, Geol. Soc. Am. Bull., **101**: 635 – 643.
23) **Batchelor, R. A. and Bowden, P. (1985).** Petrogenetic interpretation of granitoid rock series using multicationic parameters. Chem. Geol., **48**: 43-55, Amsterdam.
24) **De La Roche, H., Letrrier, J., Granclavde, P. and Marchal, M. (1980).** A classification of plutonic and volcanic rocks using R1-R2 diagram and major elements analyses. Its relationships with current nomenclature. Chem. Geol., **29**: 183-210.
25) **El Bouseily, A. M. and El Sokkary, A. A. (1975):** The relation between Rb, Ba and Sr in granitic rocks. Chem. Geol., **16**: 207-219.
26) **Whalen, J. B., Currie, K. I. and Chappell, B.W. (1987).** A-type granites: geochemical characteristic, discrimination and petrology. Contrib. Min. Petrol., **95**: 407-419.
27) **Pirajno, F. (2010).** Hydrothermal processes and mineral systems. Springer Science, Business Media B.V., 1250p.
28) **Pearce, G., Harris, N. B. W. and Tindle, A. G. (1984).** Trace element discrimination diagrams for the tectonic interpretation of granitic rocks. J. Petrol., **25**: 217 – 235.
29) **Pearce, J. A. (1982).** Trace element characteristic of lava from destructive plate boundaries. In: Thrope R. S. (ed.) andesites. Wiley Intersciences, Chichester, 525-548.
30) **Charbonneau, B. W. and Ford, K. L. (1977).** Uranium mineralization at the base of the Windsor Group, South Maitland, Nova Scotia; Current research, Part A, Geol. Surv. Can., Paper 78-1A, pp. 419-425.
31) **Finch, W. I. (1996)**. Uranium provinces of North America – Their definition, distribution, and models. U. S. G. S. Bull., 2141 p.
32) **Nash, J. T., Granger, H. C. and Adams, S. S. (1981).** Geology and concepts of genesis of important types of uranium deposits. Econ. Geol., 75th Anniv, 63–116.
33) **Mock, R. L. and Ohmoto, H. (1997).** Nondetrital origins of uranium-bearing minerals and pyrites in Early Proterozoic quartz-pebble conglomerates of the Elliot Lake District, Ontario. Ann. V. M. Goldschmidt Conf. 2273p.
34) **Frondel, C. (1958).** Systematic mineralogy of uranium and thorium, U. S. G. S. Bull., 400p.